# Characterization of Myocardial Iron Overload by Dual-Energy Computed Tomography Compared to T2* MRI. A Phantom Study

El-Sayed H. Ibrahim, Andrew W. Bowman

*Abstract*— **Iron toxicity plays a key role in tissue damage in patients with iron overload, with induced heart failure being the main cause of death. T2*-weighted magnetic resonance imaging (MRI) has been established for evaluating myocardial iron overload with strong correlation with biopsy. The recently introduced dual-energy computed tomography (DECT) has the potential for evaluating iron overload without energy-dependent CT attenuation or tissue fat effects. This study investigates the performance of DECT for evaluating myocardial iron overload (based on images acquired at four different diagnostic imaging energies of 80, 100, 120, and 140 kVp) and compare the results to MRI T2* measurements based on DECT and MRI experiments on phantoms with calibrated iron concentrations. DECT showed high accuracy for evaluating iron overload compared to MRI T2* imaging, which might help in patient staging based on the degree of iron overload and independent of the implemented imaging energy.**

## I. Introduction

Iron toxicity plays a key role in tissue damage and organ failure in patients with iron overload. While the liver is the main organ for iron deposition, iron deposition in the heart with subsequent heart failure constitutes the main cause of death in these patients [1]. Nevertheless, early institution of chelation therapy allows for reversing the iron overload-induced cardiomyopathy [2]. Different methods have been considered for evaluating tissue iron overload, including biopsy, serum ferritin level, and superconducting quantum interference device (SQUID) [3]. However, these techniques have certain limitations. Despite being the gold standard for quantifying iron content, tissue biopsy is invasive and subject to sampling error, which precludes its routine use in the clinical setting. Serum ferritin has limited capacity for predicting iron overload and it does not show good correlation with biopsy results [4]. SQUID machines have very limited availability worldwide. Recently, T2*-weighted magnetic resonance imaging (MRI) has been established as a reliable and non-invasive technique for evaluating iron overload with strong correlation with biopsy [5-8].

The existence of iron particles disturbs the local magnetic field homogeneity, which results in reduced signal intensity on T2*-weighted MRI images. Therefore, by acquiring a series of T2*-weighted images at consecutive echo times (TE) and fitting the data to an exponentially decaying curve, the tissue transverse relaxation time constant T2*, and its reciprocal R2*, could be obtained and used for assessing iron overload. Small T2* values, suggesting high myocardial iron content, have been associated with poor ventricular function in arrhythmias [9]. Specifically, T2* values of 52 ± 16 ms (at 1.5T) have been reported for normal myocardium, with T2* < 20 ms and T2* < 10 ms indicating iron overload and severe iron overload, respectively, in the heart [9]. Nevertheless, despite its advantages, MRI has some limitations, including long scan time, MRI contraindications, and inability to quantify iron concentration greater than 300 μmol/g due to susceptibility and signal loss artifacts [10].

Computed tomography (CT) can detect iron overload due to the increase in x-ray absorption caused by the larger iron density compared to soft tissues. However, CT has limited capability for quantifying iron due to the energy-dependent variation in CT attenuation. Recently, dual-energy CT (DECT) scanners have been introduced with the capability of simultaneously acquiring two images at different energy levels [11], which makes it possible for evaluating iron overload without being affected by energy-dependent CT attenuation or tissue fat [10, 12]. Further, continuous developments in CT reconstruction algorithms and detectors technology help minimize the radiation dose significantly.

As early as 1982, Goldberg et al [13] conducted CT experiments on calibrated phantoms and two dogs using 80 and 120 kVp energies, where they showed the existence of a linear relationship between iron concentration and difference in CT numbers, which could be used to predict iron content in the liver. In another study in 1986, Sephton [14] examined the potential accuracy of CT imaging at two different energies for determining hepatic iron content using in vitro scans. A couple of years later, Leighton et al [15] examined the use of conventional CT imaging at different imaging energies for measuring iron concentration in the liver in 78 Thalassemia children. About a decade later, Oelckers and Graeff [16] conducted in situ experiments for studying the errors and fat effects on measuring iron overload in the liver using CT imaging at two different imaging energies.

Recently, Fischer et al [10] and Joe et al [17] evaluated the implementation of the newly developed DECT scanners for assessing hepatic iron overload. Fischer et al [10] used different DECT images for constructing a virtual iron concentration image of the liver based on a three-material decomposition algorithm, from which they showed the existence of linear relationship between hepatic iron content and Hounsfield Unit (HU) in the absence of fat, which provides an added value for quantifying iron content irrespective of natural variation of liver iron content. Joe et al [17] showed the existence of a linear correlation between the difference of averaged attenuation between 80 and 140 kVp and iron concentration in the liver, which could be used for diagnosing clinically important hepatic iron content with sensitivity and specificity of 80% and 90%, respectively.

E. H. Ibrahim (corresponding author) is with Mayo Clinic, Jacksonville, FL 32224, USA; phone: 904-953-6037; fax: 904-953-6581 (e-mail: ibrahim.elsayed@mayo.edu).

A. W. Bowman is with Mayo Clinic, Jacksonville, FL 32224, USA (e-mails: bowman.andrew@mayo.edu).

978-1-4244-7929-0/14/$26.00 ©2014 IEEE


**Figure 1. Picture of the phantom.** Iron concentration (in μmol/g) is identified for each vial (on the cap).

Only one study in the literature addressed the importance of DECT for evaluating myocardial iron overload [12]. Hazirolan et al [12] examined the value of DECT imaging conducted at 80/140 kVp for evaluating myocardial overload in 19 Thalassemia patients, and showed a linear correlation between HU in the septal wall and MRI T2* values.

The aim of this study is to investigate the diagnostic performance of DECT for evaluating myocardial iron overload (based on images acquired at 4 different diagnostic imaging energies of 80, 100, 120, and 140 kVp) and compare the results to MRI T2* based on DECT and MRI experiments on phantoms with calibrated iron contents.

## II. Methods

### A. Phantom Creation

Ten 50-mL gel-based vials were created from a mixture of distilled water, 0.5% agarose (Agarose Type 1, #6013; Sigma-Aldrich, St. Louis, MO, USA), and 0.085 mM MnCl2 (Sigma-Aldrich, #416479) to produce T1 and T2 values similar to those of myocardium, as previously described [18]. Different amounts of iron (ammonium iron (II) sulfate; Sigma-Aldrich, #31110) ranging from 500 mg to 4500 mg in equal increments were added to nine vials to simulate iron overload in the clinical setting; the first vial was left without iron addition to be used as a reference. The chemicals were dissolved in each vial, which were heated in a microwave for 90-120 seconds until complete dissolve of the agarose. Figure 1 shows a picture of the created phantom.

### B. MRI Experiments

The phantom was imaged on a Siemens 1.5T MRI scanner using multi-echo T2*-weighted gradient-echo (GRE) pulse sequence with the following imaging parameters: repetition time (TR) = 200 ms; TE (12 echoes) = 1-16 ms in equal increments; slice thickness = 10 mm; resolution = 2.8 × 2.8 $mm^2$; flip angle = 20°; number of averages = 1; readout bandwidth = 1953 Hz/pixel; and scan time = 19 s.

### C. DECT Experiments

The phantom was imaged on a Siemens Flash DECT scanner equipped with tin filter for improved separation of the two energy spectra. Two DECT scans were conducted

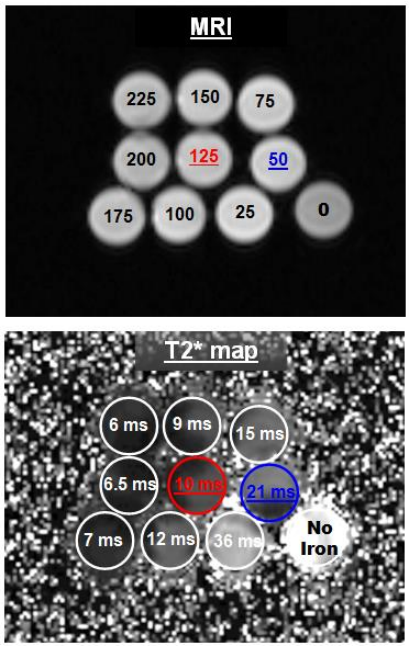


**Figure 2. MRI images of the phantom.** (a) Gradient-echo image showing iron concentration (in μmol/g) in each vial. (b) T2* map showing estimated T2* values. T2* of 21 ms (blue) and 10 ms (red) are the cutoff values. T2*<10 ms and T2*>20 ms represent severe iron overload and normal iron content, respectively.

with 80/140 kVp and 100/140 kVp energy settings. The imaging parameters were as follows: pitch = 0.6; gantry rotation time = 0.5 s ; collimation = 32×0.6 mm ; exposure time = 500 ms; tube current = 18-28 mA; slice thickness = 5 mm; resolution = 0.3 × 0.3 $mm^2$; and scan time = 2 s.

### D. Image Analysis

The images were transferred to a workstation provided by the manufacturer for analysis. A circular ROI of about 2 $cm^2$ was placed in the center of each vial to measure average signal intensity in MRI and HU in DECT.

The values from the MRI images at different TE's were fitted to a mono-exponential curve in the form of: $I = a + b \exp(-t/T2^*)$, where I is the image signal intensity; t is time; and a and b are constants. The exponential fitting resulted in T2* in ms, from which R2* (= 1000/ T2*; measured in 1/s) was calculated. Two vials resulted in T2* of 10 ms and 21 ms, which were used to study the relationship between CT energy level and HU and to construct a map for evaluating the degree of iron overload severity.

Regression and correlation analyses were conducted between iron concentration, R2*, and HU values (HU) / HU differences (ΔHU) / HU ratios (rHU) at different energies (the image at the intermediate 120 kVp energy level was calculated by the scanner from the 100/140 kVp scan).

## III. Results

### A. MRI Results

Figure 2 shows a GRE MRI image of the phantom, as well as the generated T2* map. T2* (R2*) ranged from 36 to 6 ms (28 to 167 $s^{-1}$) for iron concentrations between 25 and 225 μmol/g, respectively.

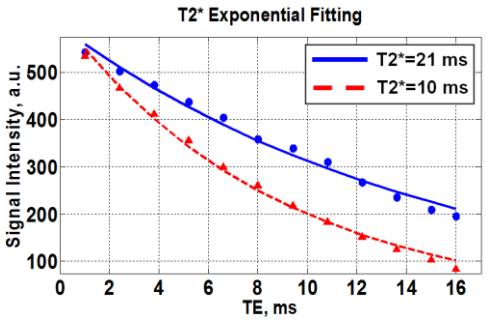


**Figure 3. T2* measurement.** Exponential fittings of the relaxation curves versus TE for vials with T2* of 21 ms (solid blue) and 10 ms (dashed red), representing the cutoffs for identifying iron overload and severe overload, respectively.

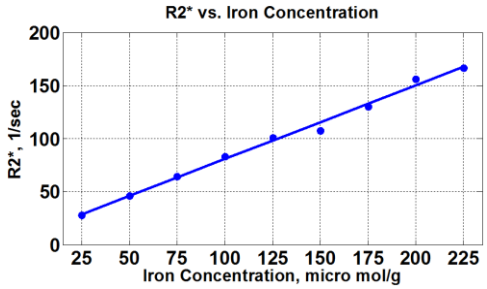


**Figure 4. R2* as an estimator of iron concentration.** There is a linear relationship between iron concentration and R2*.

Figure 3 shows the exponential curve fitting for calculating T2* of the vials with T2* of 21 and 10 ms, which represent the cutoff values for identifying iron overload and severe iron overload, respectively.

Figure 4 shows the relationship between R2* and iron concentration. The results show a strong linear correlation ($r > 0.95$ and $P < 0.0001$) between iron concentration and R2*, with linear least-squares fitting given by the equation: $y = 0.694x + 11.32$.

### *B. DECT Results*

Figure 5 shows the DECT images at different imaging energies, with varying CT attenuation depending on the iron concentration and energy level.

Figure 6 shows the relationship between HU values and iron concentration at different energy levels. The results show strong linear correlation ($r > 0.95$ and $P < 0.0001$) between iron concentration and HU at all energy levels, with linear least-squares fitting given by the equations: $y = 0.687x + 0.59$; $y = 0.562x - 0.67$; $y = 0.45x + 0.13$; and $y = 0.338x + 0.47$, for the 80, 100, 120, and 140 kVp energies, respectively.

The results showed strong linear correlation ($r > 0.95$ and $P < 0.0001$) between iron concentration and all ΔHU; and moderate linear correlations ($0.42 < |r| < 0.76$ and $0.02 < P < 0.2$) between iron concentration and rHU (except for the 140/80 ratio). Finally, R2* showed a strong linear correlation with HU values at all energy levels ($r > 0.95$ and $P < 0.001$).

The HU values of the two vials with R2* of 21 and 10 ms showed perfect linear relationships with the energy level (E), given by $HU = -0.29 \times E + 56.3$ and $HU = -0.76 \times E + 151.8$

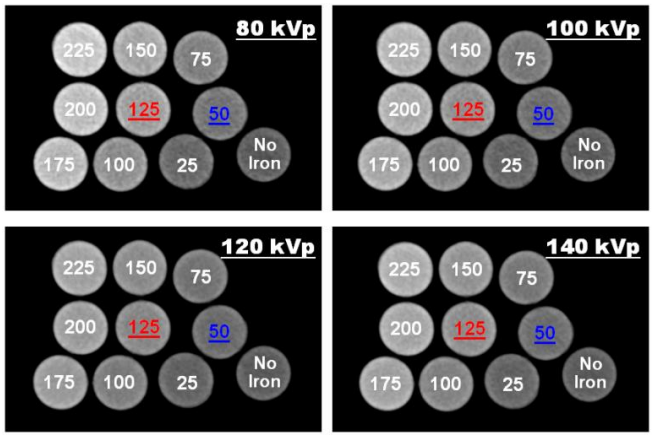


**Figure 5. CT images at 80, 100, 120, and 140 kVp.** Iron concentration (in μmol/g) is identified for each vial.

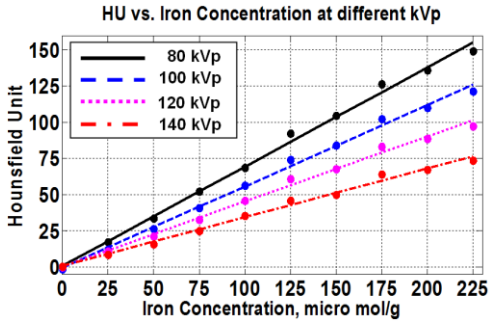


**Figure 6. Hounsfield Unit (HU) versus iron concentration.** There are linear relationships between HU and iron concentrations at different energy levels.

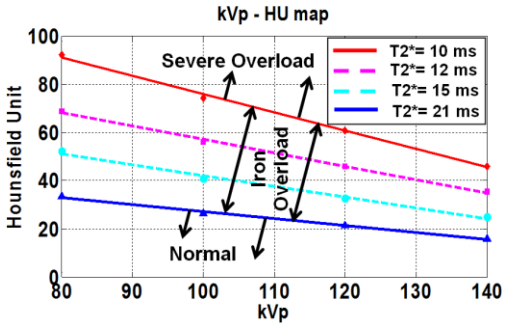


**Figure 7. CT attenuation versus energy level.** There are linear relationships between Hounsfield Unit (HU) and energy level for the iron vials that resulted in T2* between 10 ms (red) and 21 ms (blue). The figure can be used as a map to identify the severity of iron overload based on the resulting HU value and implemented kVp. Three regions can be identified on this map representing tissues with normal iron content (region below the blue line), iron overload (region between the blue and red lines), and severe iron overload (region above the red line).

for the 21 and 10 ms values, respectively, as shown in Figure 7. The resulting map can be used to evaluate the severity of iron overload by dividing the figure into three regions (normal, iron overload, and severe iron overload) based on the energy level and HU value.

## IV. Discussion

Iron toxicity plays a key role in tissue damage and organ failure in patients with iron overload, with induced heart failure being the main cause of death. MRI T2* imaging has been established for evaluating iron overload at 1.5T, despite a number of limitations, including long scan time and incapability of assessing heavy iron overload. DECT has recently been introduced with the capability of simultaneously acquiring two CT images at different energies without misregistration problems, which makes it possible for evaluating iron overload without being affected by energy-dependent CT attenuations. These capabilities make DECT a potential alternative modality for assessing tissue iron overload, especially with ongoing technological developments for minimizing radiation dose (few mSv).

This study investigated the capabilities of DECT for assessing myocardial iron overload in calibrated phantoms with different iron concentrations, and compared the results to MRI T2*. The results showed the capability of DECT for evaluating iron overload in the clinical setting with similar accuracy to that of MRI T2* imaging technique. Although the DECT HU and ΔHU values were good predictors of the degree of iron overload, rHU was not as good.

One advantage of phantom studies is the capability of generating materials with different iron concentrations similar to those in the clinical range of interest. Especially, the two vials in this study with T2* of 21 and 10 ms were very useful for creating a map for evaluating the degree of iron overload from DECT images independent of the energy level used for imaging. However, it should be noted that inherent to the nature of ex vivo studies, the proposed technique may require additional optimization for in vivo implementation.

Future work includes implementing the developed technique on a large number of patients with wide range of iron overload to investigate its clinical importance for evaluating iron overload in different diseases (e.g. thalassemia and sickle cell disease), optimize the imaging parameters for clinical implementation, and assess the technique's sensitivity and specificity.

## V. Conclusions

DECT can be used for evaluating myocardial iron overload irrespective of the implemented imaging energy with high accuracy comparable to those from MRI T2* mapping. Therefore, DECT might help in patient staging and treatment monitoring based on the severity of iron overload, without being affected by the implemented imaging energy. The low radiation dose of the imaging protocols on new scanners, very short scan time, capability of identifying large iron concentrations, and high resolution of DECT make it a promising tool for evaluating myocardial iron overload.

## References


[1] J. B. Porter, "Concepts and goals in the management of transfusional iron overload," American journal of hematology, vol. 82, pp. 1136-9, Dec 2007.

[2] P. Wacker, D. S. Halperin, D. Balmer-Ruedin, I. Oberhansli, and M. Wyss, "Regression of cardiac insufficiency after ambulatory intravenous deferoxamine in thalassemia major," Chest, vol. 103, pp. 1276-8, Apr 1993.

[3] S. Mavrogeni, "Evaluation of myocardial iron overload using magnetic resonance imaging," Blood transfusion = Trasfusione del sangue, vol. 7, pp. 183-7, Jul 2009.

[4] A. Kolnagou, C. Economides, E. Eracleous, and G. J. Kontoghiorghes, "Low serum ferritin levels are misleading for detecting cardiac iron overload and increase the risk of cardiomyopathy in thalassemia patients. The importance of cardiac iron overload monitoring using magnetic resonance imaging T2 and T2*," Hemoglobin, vol. 30, pp. 219-27, 2006.

[5] B. Cheong, S. Huber, R. Muthupillai, and S. D. Flamm, "Evaluation of myocardial iron overload by T2* cardiovascular magnetic resonance imaging," Texas Heart Institute journal, vol. 32, pp. 448-9, 2005.

[6] L. J. Anderson, S. Holden, B. Davis, E. Prescott, C. C. Charrier, N. H. Bunce, D. N. Firmin, B. Wonke, J. Porter, J. M. Walker, and D. J. Pennell, "Cardiovascular T2-star (T2*) magnetic resonance for the early diagnosis of myocardial iron overload," European heart journal, vol. 22, pp. 2171-9, 2001.

[7] M. A. Westwood, D. N. Firmin, M. Gildo, G. Renzo, G. Stathis, K. Markissia, B. Vasili, and D. J. Pennell, "Intercentre reproducibility of magnetic resonance T2* measurements of myocardial iron in thalassaemia," The international journal of cardiovascular imaging, vol. 21, pp. 531-8, Oct 2005.

[8] A. K. Kondur, T. Li, P. Vaitkevicius, and L. Afonso, "Quantification of myocardial iron overload by cardiovascular magnetic resonance imaging T2* and review of the literature," Clinical cardiology, vol. 32, pp. E55-9, Jun 2009.

[9] D. J. Pennell, "T2* magnetic resonance and myocardial iron in thalassemia," Annals of the New York Academy of Sciences, vol. 1054, pp. 373-8, 2005.

[10] M. A. Fischer, C. S. Reiner, D. Raptis, O. Donati, R. Goetti, P. A. Clavien, and H. Alkadhi, "Quantification of liver iron content with CT-added value of dual-energy," European radiology, vol. 21, pp. 1727-32, Aug 2011.

[11] M. Petersilka, H. Bruder, B. Krauss, K. Stierstorfer, and T. G. Flohr, "Technical principles of dual source CT," European journal of radiology, vol. 68, pp. 362-8, 2008.

[12] T. Hazirolan, B. Akpinar, S. Unal, F. Gumruk, M. Haliloglu, and S. Alibek, "Value of Dual Energy Computed Tomography for detection of myocardial iron deposition in Thalassaemia patients: initial experience," European journal of radiology, vol. 68, pp. 442-5, 2008.

[13] H. I. Goldberg, C. E. Cann, A. A. Moss, M. Ohto, A. Brito, and M. Federle, "Noninvasive quantitation of liver iron in dogs with hemochromatosis using dual-energy CT scanning," Investigative radiology, vol. 17, pp. 375-80, 1982.

[14] R. G. Sephton, "The potential accuracy of dual-energy computed tomography for the determination of hepatic iron," The British journal of radiology, vol. 59, pp. 351-3, Apr 1986.

[15] D. M. Leighton, J. F. de Campo, R. Matthews, and R. G. Sephton, "Dual energy CT estimation of liver iron content in thalassaemic children," Australasian radiology, vol. 32, pp. 214-9, May 1988.

[16] S. Oelckers and W. Graeff, "In situ measurement of iron overload in liver tissue by dual-energy methods," Physics in medicine and biology, vol. 41, pp. 1149-65, Jul 1996.

[17] E. Joe, S. Kim, K. B. Lee, J. J. Jang, J. Y. Lee, J. M. Lee, J. K. Han, and B. I. Choi, "Feasibility and accuracy of dual-source dual-energy CT for noninvasive determination of hepatic iron accumulation," Radiology, vol. 262, pp. 126-35, 2012.

[18] S. H. Ibrahim el, F. N. Rana, K. R. Johnson, and R. D. White, "Assessment of cardiac iron deposition in sickle cell disease using 3.0 Tesla cardiovascular magnetic resonance," Hemoglobin, vol. 36, pp. 343-61, 2012.